Single-neutron removal from ^{14,15,16}C near 240 MeV/nucleon

Y. Z. Sun,[1] S. T. Wang,[2,3,*] Z. Y. Sun,[2,3] X. H. Zhang,[2,3] S. Y. Jin,[2,3,4] Y. X. Zhao,[2,3,4] D. Y. Pang,[5] S. W. Tang,[2,3] D. Yan,[2] P. Ma,[2] Y. H. Yu,[2,3] K. Yue,[2] F. Fang,[2] Y. J. Zhang,[2] C. G. Lu,[2] and L. M. Duan[2,3]

[1]*School of Physics and Electrical Engineering, Anyang Normal University, Anyang 455000, China*

[2]*CAS Key Laboratory of High Precision Nuclear Spectroscopy, Institute of Modern Physics, Chinese Academy of Sciences, Lanzhou 730000, China*

[3]*School of Nuclear Science and Technology, University of Chinese Academy of Sciences, Beijing 100049, China*

[4]*School of Nuclear Science and Technology, Lanzhou University, Lanzhou 730000, China*

[5]*School of Physics and Nuclear Energy Engineering, Beihang University, Beijing 100191, China*

(Received 31 March 2021; revised 21 May 2021; accepted 24 June 2021; published 12 July 2021)

A consistent measurement of the inclusive single-neutron removal cross sections of ^{14,15,16}C on a carbon target at around 240 MeV/nucleon has been performed at the External Target Facility, HIRFL-CSR, and compared with Glauber model predictions using shell-model spectroscopic strengths between the initial projectile ground state and configurations of bound core state + valence neutron state as input. For the dependence of the spectroscopic factor reduction characterized by the ratio R_s of the experimental over theoretical single-nucleon removal cross section on the bounding depth ΔS of the removed nucleon established in single-nucleon removals with beam energies mainly over 80–120 MeV/nucleon, our measurement gives R_s values that conform to the earlier R_s-ΔS systematics, where the relatively higher incident beam energy facilitates the applicability of the eikonal and sudden approximation used in the Glauber model.

DOI: 10.1103/PhysRevC.104.014310

I. INTRODUCTION

Residual interactions originated from internucleon correlations introduce configuration mixing to an independent particle model description of atomic nuclei. The spectroscopic strengths of different configurations of nucleons in a nuclear many-body wave function carry significant information about nucleon-nucleon correlations and single-particle structures of the nucleus and enter eikonal reaction models as nuclear structure inputs in the calculation of single-nucleon removal cross sections to be compared with experimental measurements [1], serving as an estimator of the effective interactions used in nuclear shell models.

Experimentally, direct removal (knockout) of one nucleon from stable or radioactive ion beams (RIB) ranging from tens of to several hundred of MeV/nucleon has been widely used for nuclear spectroscopy since the beginning of the 21st century [1]. The inclusive single-nucleon removal cross section σ is related to nuclear spectroscopic factors C^2S via Eq. (1) [2]:

$$\sigma = \sum_{nlj} \left(\frac{A}{A-1}\right)^N C^2S(\alpha, nlj)\sigma_{\rm sp}(nlj, S^*_\alpha), \qquad (1)$$

where σ is calculated as the sum of partial reaction cross sections of a mass A projectile populating a mass $A-1$ core bound state α after a nucleon is removed from a single-particle orbital nlj. $S^*_\alpha = S_{n(p)} + E^*_\alpha$ is the effective separation energy, with $S_{n(p)}$ being the ground-state (g.s.) to g.s. nucleon separation energy of valence neutron (proton), and E^*_α is the energy of the core state α with respect to its ground state. C^2S is the shell-model spectroscopic factor corresponding to the nucleon-removal channel, calculated as the wave-function overlap following Eq. (2) [1]:

$$\begin{aligned} \left\langle \vec{r}, \Psi^{A-1}_\alpha \middle| \Psi^A_{\rm g.s.} \right\rangle &= \sum_{nlj} c_{nlj,\alpha}\psi_{nlj}(\vec{r}), \\ C^2S(\alpha, nlj) &= |c_{nlj,\alpha}|^2. \end{aligned} \qquad (2)$$

The $[A/(A-1)]^N$ factor preceding C^2S in Eq. (1) is a center-of-mass correction [3], where $N = 0, 1, 2\ldots$ is the major oscillator quantum number when C^2S is calculated in a harmonic-oscillator basis. $\sigma_{\rm sp}(nlj, S^*_\alpha)$ is the so-called single-particle (sp) cross section, calculated using reaction models assuming a normalized valence nucleon-core relative wave function ψ_{nlj}. The Glauber model [4] is widely used for the calculation of $\sigma_{\rm sp}$. The theory is based on sudden and eikonal (SE) approximation, which uses the eikonal valence nucleon-core relative wave function ψ_{nlj} and treats the core nucleus as a spectator during the nucleon-removal process. So beam energy being large enough is crucial for the basis of the Glauber model to be valid [5].

Accumulated experimental data show that single-nucleon removal cross sections σ are universally overestimated by the Glauber model with shell-model structure inputs [6]. Defining the ratio of experimental over theoretical values of σ, $R_s = \sigma_{\rm exp}/\sigma_{\rm th}$, and the asymmetry of the neutron and proton Fermi surfaces ΔS (isospin asymmetry, see Sec. IV), it is found that R_s drops almost linearly with respect to ΔS, as shown by Fig. 1 of Ref. [6]. Note that data points therein are obtained with beam energies mainly over 80–120 MeV/nucleon and

*wangshitao@impcas.ac.cn

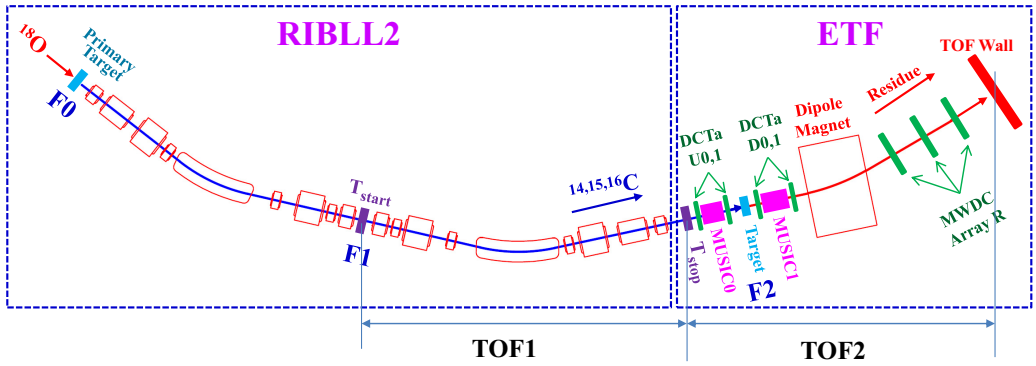

FIG. 1. A schematic view (not to scale) of RIBLL2 and ETF. TOF1 and TOF2 mark the flight paths of the time-of-flight measurements. $T_{\rm start}$, $T_{\rm stop}$, and TOF Wall are all plastic scintillators for TOF measurements.

from separate experiments with their own systematic errors, and because high beam energy enhances the applicability of the SE approximation, it is interesting to enhance the R_s-ΔS dependence with consistent measurements of σ at a considerably higher beam energy.

This idea becomes more appealing as the R_s-ΔS dependence is contradicted by systematic study of R_s with (p, d) transfer reactions [7,8] and quasifree $(p, 2p)$ reactions [9,10] over a large span of isospin asymmetry. They both observed weak or no dependence of R_s on ΔS despite the difference in reaction mechanisms. The hydrogen target may play a vital part, in comparison with the composite target (usually beryllium or carbon) used in knockout reactions, where the target nuclei take larger sizes and possess internal nuclear structure, and so may have a higher probability to excite the core to unbound state, resulting in reaction cross section loss, especially for removal of deeply bound nucleons. Because the choice of target nuclei is irrelevant to beam energy, this plausible explanation would be excluded if R_s observed in knockout reactions at higher beam energies showed little dependence on ΔS.

R_s extracted from knockout reactions with a variety of beam energies ($E_{\rm b}$) will also provide significant data to improve the Glauber model in its incident-energy-dependent part. It is a common practice (as is adopted in this work) to represent the interaction between the target and the mass $A-1$ core (or valence nucleon) using the so-called t-ρ-ρ method [4], where incident-energy dependence of the scattering S matrix is introduced by using free nucleon-nucleon scattering cross sections fitted to experimental data as a function of the incident energy. This treatment ignores the possibility that beams with higher energies may dig deeper into the nuclei, where the struck nucleon may experience stronger internucleon correlations [11], which in turn manifests itself as R_s-$E_{\rm b}$ dependence. Accumulated systematic experimental data over a wide beam-energy range will verify this effect and provide a corresponding benchmark for reaction models like the Glauber model. There are experimental data for single-neutron removal from neutron-rich carbon isotopes at 50–103 MeV/nucleon [12,13] and 700 MeV/nucleon [14], which makes them a good option for the study of R_s-$E_{\rm b}$ dependence.

This paper reports single-neutron removal cross sections from ^{14,15,16}C on a carbon target at around 240 MeV/nucleon. The experimental setup and extraction of reaction cross sections are described, followed by interpretation of σ with theoretical results and finally the obtained R_s-ΔS dependence.

II. EXPERIMENT

The experiment was conducted at the External Target Facility (ETF [15]) of the Heavy Ion Research Facility in Lanzhou [16]-Cooler Storage Ring [17] (HIRFL-CSR). Primary ^{18}O beams were accelerated to 280 MeV/nucleon by HIRFL-CSR and fragmented on a 15-mm-thick Be target. The generated secondary beams were subsequently selected by their magnetic rigidities in the second Radioactive Ion Beam Line in Lanzhou (RIBLL2 [18]) and then delivered to ETF to impinge on a 900-mg/cm^2 carbon target, where their energies dropped to around 240 MeV/nucleon upon hitting the target. Beam energies at the middle of the reaction target were 239, 237, and 235 MeV/nucleon for ^{16}C, ^{15}C, and ^{14}C, respectively. The setups of RIBLL2 and ETF are illustrated in Fig. 1. The secondary beams were identified using the ΔE-TOF method, with the time of flight (TOF) shown as TOF1 in Fig. 1 representing the incident particle's mass over charge ratio A/Z (aoz) and with ΔE_0 measured by the multisampling ionization chamber (MUSIC0 [19]) upstream from the reaction target giving the particle's charge number Z. RIBLL2 has achieved satisfying particle identification (PID), as exhibited by Fig. 2 for the delivery of the ^{15}C beam.

Reaction products downstream from the reaction target were identified via $B\rho$-ΔE-TOF method following Eq. (3):

$$B\rho \propto p/Z \propto A/Z \cdot \beta\gamma, \tag{3}$$

where p is the momentum, A is the particle mass number, γ is the Lorentz factor, and $B\rho$ is the magnetic rigidity, calculated from particle tracks. The particle Z number was recorded by MUSIC1 [20] downstream from the reaction target, while the particle TOF (TOF2) were given by the plastic scintillators $T_{\rm stop}$ [21] and the TOF Wall [22] (see Fig. 1). The heavy reaction products were traced via a series of drift chambers, lined up along the particles' flying directions as DCTaD0,1 and DC0,1,2, with the latter constituting the MWDC Array R [23] (see Fig. 1). The MWDC Array R and the TOF Wall system featured large geometrical acceptance. Reconstructed two-dimensional position distribution of the reaction products

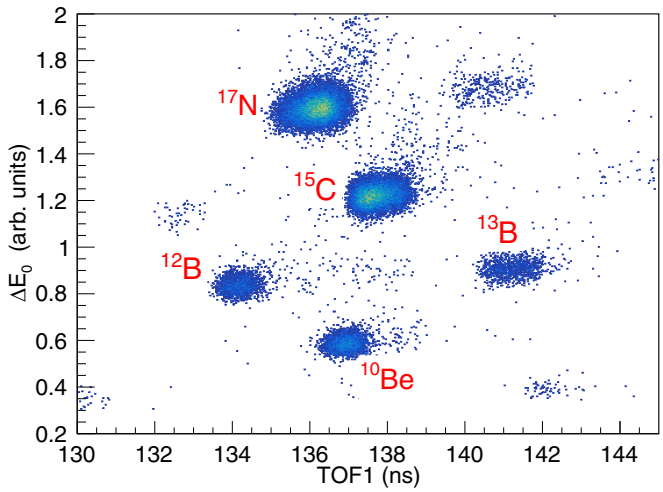

FIG. 2. Particle identification spectrum of RIBLL2 using the ^{15}C setting.

on the sensitive areas of the detectors indicates that the heavy residues from single-neutron removal have been fully included in the detecting system.

The obtained PID spectrum for neutron-removal products of incident ^{15}C is shown in Fig. 3, with an achieved *aoz* resolution $\sigma_{aoz}/aoz \approx 0.01$. It can be seen from Fig. 3 that the single-neutron removal product is clearly separated from the incident nuclei, though there is still a perceptible presence of ^{15}C's *aoz* tail blended in ^{14}C. Data analysis indicates that the *aoz* tails originate from tracking deficiencies of the detectors [24]. We therefore treat as target independent the contamination of the unreacted nuclei propagating into the region of its single-neutron removal product. It is supposed to be canceled out by target-out subtraction. Denoting $aoz_{\min}$ as the *aoz* local minimum point where the *aoz* peaks of the unreacted nuclei and the single-neutron removal product meet in the PID spectrum, the *aoz* range for single-neutron removal product is chosen so that $aoz \leqslant aoz_{\min}$. Yield loss due to the tails excluded from the *aoz* cut is compensated for by assuming the single-neutron removal products have the same probability distribution as the unreacted nuclei for the *aoz* tails in the PID spectrum.

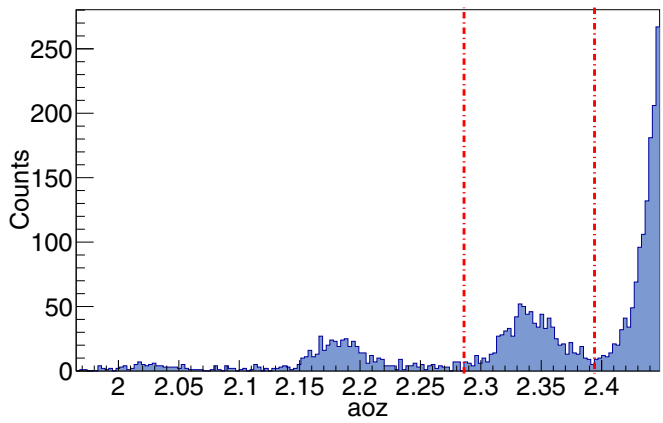

FIG. 3. An *aoz* profile of ^{15}C and its neutron removal products. The red dash-dotted lines mark the *aoz* range chosen for ^{14}C, which is centered at the mean value of a Gaussian fit to the peak in the range.

TABLE I. Single-neutron removal cross sections including target-in σ_{TAin}, target-out σ_{TAout}, and final σ_{exp} for ^{14}C, ^{15}C, and ^{16}C impinging on a carbon target at around 240 MeV/nucleon, together with the detecting efficiencies ϵ_{d} and the compensation factors $\epsilon^{\mathrm{SV}}_{\mathrm{TAin}}$ and $\epsilon^{\mathrm{SV}}_{\mathrm{TAout}}$ for the target-thickness effect in target-in and target-out runs. The cross sections are in mb. All the errors are statistical.

Reaction	(^{16}C, ^{15}C)	(^{15}C, ^{14}C)	(^{14}C, ^{13}C)
σ_{TAin}	187(6)	270(9)	196(6)
σ_{TAout}	104(6)	162(7)	116(4)
σ_{exp}	83(8)	108(11)	80(7)
ϵ_{d}	0.908(5)	0.908(4)	0.913(3)
$\epsilon^{\mathrm{SV}}_{\mathrm{TAin}}$	0.946(5)	0.944(5)	0.959(3)
$\epsilon^{\mathrm{SV}}_{\mathrm{TAout}}$	0.983(6)	0.983(5)	0.988(4)

III. EXTRACTION OF SINGLE-NEUTRON REMOVAL CROSS SECTION

The reaction cross section for a general reaction channel i is calculated according to Eq. (4):

$$\sigma_i = \frac{\Delta N_i}{N_0 t \epsilon}, \tag{4}$$

where ΔN_i is the count of the objective residue, N_0 is the incident particle number, t is the target nucleus density per area, and ϵ is the PID efficiency accounting for detecting efficiency, geometrical efficiency, and compensation for reaction cross section loss due to the interaction of incident particles and heavy residues with the target nuclei while making their way through the target (target-thickness effect). The contribution to σ_i from reactions other than those in the reaction target is evaluated from target-out runs and subtracted. As has been mentioned in Sec. II, the geometrical efficiency is taken to be 100%. The detecting efficiency ϵ_{d} is extracted from target-out runs as the probability that a particle flying through the sensitive area of the post-target-detecting system gets successfully PIDed.

The cross sections for the target-in σ_{TAin}, the target-out σ_{TAout}, and the final σ_{exp} are listed in Table I, together with their detecting efficiencies ϵ_{d} and the compensation factors $\epsilon^{\mathrm{SV}}_{\mathrm{TAin}}$ and $\epsilon^{\mathrm{SV}}_{\mathrm{TAout}}$ for the target-thickness effect in target-in and target-out runs.

Note that while the *aoz* of the incident particles are identified before passing through T_{stop} (see Fig. 1), products of neutron-removal process happened within the 3-mm-thick T_{stop} cannot be distinguished from the incident nuclei and are treated as backgrounds, which accounts for the relative large empty-target cross sections of the single-neutron removal channel and the nontrivial values of $\epsilon^{\mathrm{SV}}_{\mathrm{TAout}}$. Because the detecting process of the detectors is electromagnetic, we ignore the difference of detecting efficiencies between the incident nuclei and its neutron-removal products. The difference in ϵ_{d} between incident ^{14}C, ^{15}C, and ^{16}C was dominated by fluctuations in detector working conditions among individual

TABLE II. Single-nucleon removal cross sections of ^{14,15,16}C impinging on a carbon target at 235, 237, and 239 MeV/nucleon, respectively. $(E^*_\alpha I^\pi_c + nlj)$ represent core + valence neutron configurations in the projectile ground state. $\sigma_{\rm th}$'s are the theoretical inclusive single-neutron removal cross sections calculated using MOMDIS with C^2S taken from Refs. [12,28]. $\Delta S = S_n + \bar{E}^* - S_p$ is the asymmetry of the neutron and proton Fermi surfaces for the removed neutron, where $\bar{E}^*$ is the averaged core excitation energy over each final core state weighted by the calculated partial cross section to that state. $\sigma_{\rm exp}$'s are the experimental results of this work. $R_s = \sigma_{\rm exp}/\sigma_{\rm th}$ is the reduction factor of the spectroscopic factor. All the errors are statistical.

Reaction	E^*_α	I^π_c	nlj	C^2S	$\sigma_{\rm th}$ (mb)	$\sigma_{\rm exp}$ (mb)	R_s
(^{16}C, ^{15}C)	0.000	$1/2^+$	$1s_{1/2}$	0.601	33.4		
$\Delta S^{\rm eff} = -17.9$ MeV	0.740	$5/2^+$	$0d_{5/2}$	1.232	44.8		
	Inclusive				78.3	83(8)	1.06(11)
(^{15}C, ^{14}C)	0.000	0^+	$1s_{1/2}$	0.978	90.6		
$\Delta S^{\rm eff} = -17.6$ MeV	6.094	1^-	$0p_{3/2}$	1.180	36.6		
	6.903	0^-	$0p_{1/2}$	0.459	13.7		
	7.012	2^+	$0d_{5/2}$	0.020	0.7		
	Inclusive				141.6	108(11)	0.76(8)
(^{14}C, ^{13}C)	0.000	$1/2^-$	$0p_{1/2}$	1.67	53.6		
$\Delta S^{\rm eff} = -10.8$ MeV	3.684	$3/2^-$	$0p_{3/2}$	2.05	56.8		
	Inclusive				110.4	80(7)	0.73(7)

experiment runs. The reaction cross-section extraction technique is formulated in more detail in Ref. [25].

IV. RESULTS AND DISCUSSION

The computer code MOMDIS [26] implementing the Glauber model for knockout reactions is employed to calculate the single-neutron knockout cross section $\sigma_{\rm sp}(nlj, S^*_\alpha)$. The code requires nucleon density distributions of the core and the target as input, which are calculated with Hartree-Fock calculations based on the SkX parametrization [27]. The valence neutron-core relative wave function ψ_{nlj} for each (α, nlj) configuration is calculated using the Woods-Saxon (WS) potential with $r_0 = 1.25$ fm and $a = 0.7$ fm, as in Refs. [2,28]. The depths of the WS potentials are adjusted to reproduce the effective separation energy $S^*_\alpha = S_n + E^*_\alpha$. As has been mentioned in Sec. I, we have used the t-ρ-ρ method to build the optical potentials between target nuclei and the mass $A - 1$ core (or the valence neutron), with Horiuchi parametrization for free nucleon-nucleon scattering cross sections [29]. The theoretical prescription is consistent with Ref. [2], but slightly different from what has been adopted in Ref. [6], which uses the Ray parametrization [30] instead of the Horiuchi one and r_0 constrained by the rms radius of the sp orbital of the valence nucleon given by Hartree-Fock (HF) calculations. Horiuchi parametrization is preferred in this work for it covers a wider energy range (30 to 1000 MeV/u) and gives a better agreement with experimental data [2]. The differences between single-neutron removal $\sigma_{\rm th}$ calculated using $r_0 = 1.25$ fm and r_0 ($r_0^{\rm HF}$) obtained in the manner of Ref. [6] are estimated with $r_0^{\rm HF}$ reported in Ref. [13] for ^{15}C. The use of $r_0^{\rm HF}$ leads to a 8.4% drop in the $\sigma_{\rm th}$, smaller than the uncertainty in the experimental cross section (10.6%).

Spectroscopic factors of the neutron-removal reaction $C^2S(\alpha, nlj)$ and the level energies of the residue final states E^*_α are required to calculate the inclusive single-neutron removal cross sections $\sigma_{\rm th}$ according to Eq. (1). There exist several sets of $C^2S(\alpha, nlj)$ and E^*_α in the literature for ^{14,15,16}C that differ slightly from each other [2,12,13,28]. We have adopted $C^2S(\alpha, nlj)$ calculated with the WBP interaction [31] from Refs. [12,28] for ^{15,16}C and ^{14}C, respectively. With the model inputs described above, $\sigma_{\rm th}$ cross sections are calculated and tabulated in Table II, together with the experimental cross sections $\sigma_{\rm exp}$ extracted in this work. The asymmetry of the neutron and proton Fermi surfaces for the removed neutron is calculated as $\Delta S = S_n + \bar{E}^* - S_p$, where $\bar{E}^*$ is the averaged core excitation energy over each final bound core state weighted by the calculated partial cross section to that state.

The data listed in Table II enable us to catch a glimpse of the behavior of R_s-ΔS dependence at a considerably

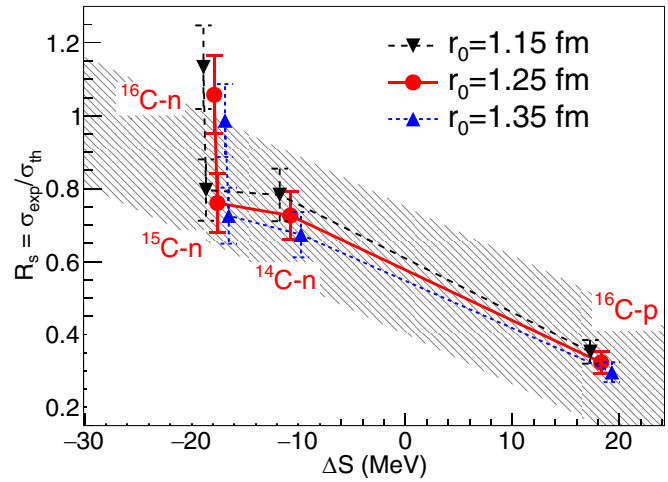

FIG. 4. The R_s-ΔS dependence obtained with $r_0 = 1.15$, 1.25, and 1.35 fm for single-neutron removal of ^{14}C, ^{15}C, and ^{16}C and single-proton removal of ^{16}C at around 240 MeV/nucleon on a carbon target taken from Ref. [32]. ΔS for $r_0 = 1.15$ fm (1.35 fm) are applied to by an offset of -1 MeV/nucleon ($+1$ MeV/nucleon) for convenience of comparison. The lines are to guide the eyes. The hatched area summarizes the totality of the data points from Fig. 1 of Ref. [6].

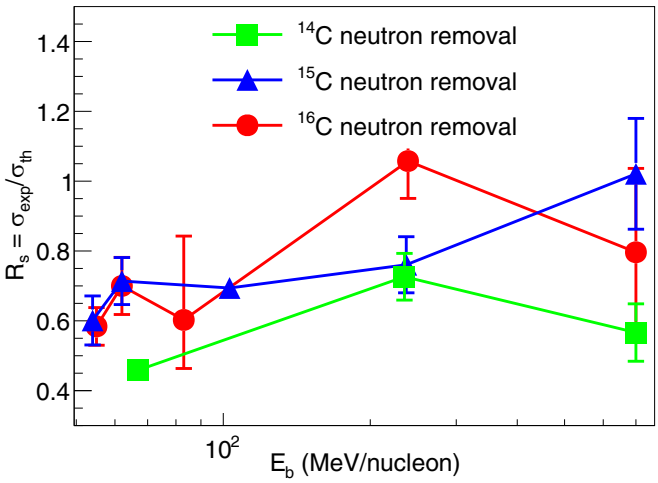

FIG. 5. R_s as a function of incident energy E_b for single-neutron removal from ^{14,15,16}C on carbon and beryllium targets. Data points at around 240 MeV/nucleon are from this work. See text for the references of other data.

higher level of incident energy with consistent experimental conditions and theoretical inputs. The three points using $r_0 = 1.25$ fm are drawn in Fig. 4, which are also joined by a reported single-proton removal cross section of ^{16}C at 239 MeV/nucleon [32]. The hatched band in Fig. 4 summarizes the totality of the data points in Fig. 1 of Ref. [6].

Figure 4 shows that the R_s-ΔS dependence established with beam energies mainly over 80–120 MeV/nucleon still holds for beam energies up to around 240 MeV/nucleon, where it facilitates the applicability of the SE approximation for the Glauber model. The resilience of the R_s-ΔS dependence against the beam energy indicates that the reason behind this nearly linear decrease of R_s along ΔS is not dominated by possible energy dependence of the validity of the SE approximation. We have also noticed that the central values of R_s are scattered around the formerly established systematics. More experiments over this beam energy region are needed to confirm this.

We have tried to rule out the uncertainties brought about by theoretical inputs to the R_s-ΔS systematics obtained here. Because, of all the input parameters, the calculated cross sections are particularly sensitive to r_0 of the WS potentials between the core and the valence neutron [33], following Ref. [32], the r_0's used in MOMDIS are varied by ± 0.1 fm to regain R_s-ΔS data points, which are also drawn in Fig. 4. While the σ_{th} values change correspondingly by $\sim\pm 7\%$, the R_s-ΔS systematics barely changes.

Finally, to inspect the R_s-E_b dependence, Fig. 2 of Ref. [2] is supplemented with σ_{exp} of this work and ^{14}C at 67 MeV/nucleon [12] and 700 MeV/nucleon [14]. The updated figure is represented in Fig. 5. The other data points in the figure are ^{15}C at 54, 62, and 85 MeV/nucleon, ^{16}C at 55, 62, and 83 MeV/nucleon on a carbon target [12], ^{15}C at 103 MeV/nucleon on a beryllium target [13], and ^{15,16}C at 700 MeV/nucleon on a beryllium target [14]. For data points at 700 MeV/nucleon, only ^{16}C has implemented empty-target cross-section subtraction. An average correction factor is applied to σ_{exp} in place of the empty-target correction [2]. More details are found in Ref. [2]. Figure 5 does not exhibit strong beam-energy dependence of R_s. Good consistency is seen for ^{15}C at different incident energies given the statistical and potential systematic errors.

V. CONCLUSIONS

Inclusive single-neutron removal cross sections for ^{14,15,16}C on a carbon target at around 240 MeV/nucleon are extracted consistently to reexamine the isospin asymmetry dependence of the reduction factor $R_s = \sigma_{exp}/\sigma_{th}$. The R_s-ΔS dependence obtained in this work is in line with that established for beam energies mainly over 80–120 MeV/nucleon, which indicates that the beam-energy dependence of the applicability of the SE approximation plays a minor role. The reduction factors R_s for single-neutron removal of ^{14,15,16}C at several beam energies E_b over 50 to 240 MeV/nucleon and 700 MeV/nucleon also show no strong R_s-E_b dependence, consistent with the above conclusion.

ACKNOWLEDGMENTS

We are obliged to the crew of HIRFL-CSR for providing high-quality beams. This project was funded by the National Natural Science Foundation of China (Grants No. U1732134, No. 11575257, and No. 11305222), the Key Laboratory of High Precision Nuclear Spectroscopy, the Institute of Modern Physics, the Chinese Academy of Sciences, and the Open Research Project of CAS Large Research Infrastructures.

[1] P. G. Hansen and J. A. Tostevin, Annu. Rev. Nucl. Part. Sci. **53**, 219 (2003).
[2] C. Wen *et al.*, Chin. Phys. C **41**, 054104 (2017).
[3] A. Dieperink and T. de Forest, Phys. Rev. C **10**, 543 (1974).
[4] C. Bertulani and P. Danielewicz, *Introduction to Nuclear Reactions* (CRC, Boca Raton, FL, 2004), p. 428.
[5] F. Flavigny, A. Obertelli, A. Bonaccorso, G. F. Grinyer, C. Louchart, L. Nalpas, and A. Signoracci, Phys. Rev. Lett. **108**, 252501 (2012).
[6] J. A. Tostevin and A. Gade, Phys. Rev. C **90**, 057602 (2014).
[7] J. Lee *et al.*, Phys. Rev. C **83**, 014606 (2011).
[8] J. Lee *et al.*, Phys. Rev. Lett. **104**, 112701 (2010).
[9] L. Atar *et al.* (R^{3}B Collaboration), Phys. Rev. Lett. **120**, 052501 (2018).
[10] M. Holl *et al.*, Phys. Lett. B **795**, 682 (2019).
[11] T. Aumann *et al.*, Prog. Part. Nucl. Phys. **118**, 103847 (2021).
[12] E. Sauvan *et al.*, Phys. Rev. C **69**, 044603 (2004).
[13] J. R. Terry, D. Bazin, B. A. Brown, J. Enders, T. Glasmacher, P. G. Hansen, B. M. Sherrill, and J. A. Tostevin, Phys. Rev. C **69**, 054306 (2004).
[14] C. Rodríguez-Tajes *et al.*, Phys. Rev. C **82**, 024305 (2010).
[15] Y. Z. Sun *et al.*, Nucl. Instrum. Methods Phys. Res., Sect. A **927**, 390 (2019).
[16] W. L. Zhan *et al.*, Nucl. Phys. A **805**, 533c (2008).

[17] J. W. Xia *et al.*, Nucl. Instrum. Methods Phys. Res., Sect. A **488**, 11 (2002).
[18] B. H. Sun *et al.*, Sci. Bull. **63**, 78 (2018).
[19] X. H. Zhang *et al.*, Nucl. Instrum. Methods Phys. Res., Sect. A **795**, 389 (2015).
[20] K. Kimura *et al.*, Nucl. Instrum. Methods Phys. Res., Sect. A **538**, 608 (2005).
[21] W. J. Lin *et al.*, Chin. Phys. C **41**, 066001 (2017).
[22] Y. Sun *et al.*, Nucl. Instrum. Methods Phys. Res., Sect. A **893**, 68 (2018).
[23] Y. Z. Sun *et al.*, Nucl. Instrum. Methods Phys. Res., Sect. A **894**, 72 (2018).
[24] Y. Z. Sun *et al.*, Nucl. Instrum. Methods Phys. Res., Sect. A **985**, 164682 (2021).
[25] Y. Z. Sun *et al.*, Nucl. Phys. Rev. **37**, 742 (2020).
[26] C. A. Bertulani and A. Gade, Comput. Phys. Commun. **175**, 372 (2006).
[27] B. A. Brown, Phys. Rev. C **58**, 220 (1998).
[28] E. C. Simpson and J. A. Tostevin, Phys. Rev. C **79**, 024616 (2009).
[29] W. Horiuchi, Y. Suzuki, B. Abu-Ibrahim, and A. Kohama, Phys. Rev. C **75**, 044607 (2007).
[30] L. Ray, Phys. Rev. C **20**, 1857 (1979).
[31] E. K. Warburton and B. A. Brown, Phys. Rev. C **46**, 923 (1992).
[32] Y. X. Zhao *et al.*, Phys. Rev. C **100**, 044609 (2019).
[33] A. Gade *et al.*, Phys. Rev. C **77**, 044306 (2008).